Available online at www.sciencedirect.com
SCIENCE DIRECT®
Chemical Physics 316 (2005) 72–82
Chemical Physics
www.elsevier.com/locate/chemphys

An ab initio LAPW study of the α and β phases of bulk molybdenum trioxide, MoO_3

A.D. Sayede [a,*], T. Amriou [b], M. Pernisek [b], B. Khelifa [b], C. Mathieu [b]

[a] LPCIA, CNRS-FRE 2485, Faculté des Sciences Jean Perrin, Rue Jean Souvraz, Université d'Artois, SP 18, 62307, Lens Cedex, France
[b] CCML, Faculté des Sciences Jean Perrin, Rue Jean Souvraz, Université d'Artois, SP 18, 62307, Lens Cedex, France

Received 25 April 2005; accepted 27 April 2005
Available online 13 June 2005

Abstract

Structure and electronic properties of the α and β-MoO_3, have been studied with periodic LAPW calculations. The structure and electronic properties of the α-MoO_3 are in quite agreement with experimental and previous theoretical results. The oxide is partially ionic and the symmetrically bridging oxygens exhibit more ionic feature while the terminal oxygens are more covalent. The lattice scaling of the β-MoO_3 give results in excellent agreement with the reported experimental pseudo-cubic results. It has been found from density of states (DOS) that β-MoO_3 is not fully ionic system and some covalent contributions are still appreciable. These covalent contributions to the bonding appear derisory compared to the covalent contributions of the α phase. The β-MoO_3 → α-MoO_3 transformation is explained by metal off-center displacement toward O_1 (and a little less toward O_2) centers which is stabilized by an increase in covalency between the Mo and oxygen atoms.

PACS: 71.15.Ap; 71.15.Mb

Keywords: LAPW; DFT; α-MoO_3; β-MoO_3 and electronic structure

1. Introduction

Transition metal oxides are well known for their diverse structural, physical and chemical properties [1–3]. These materials exist in many crystallographic forms with stoichiometries differing only slightly from each other and transition metal ions exhibiting various oxidation states. Among these oxides, molybdenum oxides represent an important class of system which are widely studied and used in many technological applications. In particular, molybdenum trioxide MoO_3 is an important heterogeneous catalyst [2,4,5], electrochromic component [6] and active material in secondary lithium batteries [7–11].

Molybdenum trioxide can exist in two crystalline polymorphs form, the thermodynamically stable orthorhombic α-MoO_3 [12], and the metastable monoclinic β-MoO_3 phase [13–16]. α-MoO_3 crystallizes with lattice constants $a = 13.855$ Å, $b = 3.696$ Å and $c = 3.963$ Å. It has a layer structure in which each layer is built up of MoO_6 octahedron at two levels, connected along y-axis by common edges and corners, so as to form zigzag rows and along z-axis by common corners only (see Fig. 1). Moreover each layer exhibits, in the y-axis direction, oxygen atoms which are common for three different octahedron. Each octahedra also shares, along z-axis, two oxygen atoms with two neighboring octahedron. Besides, for each MoO_6 octahedra there is only one oxygen atom which is doubly bounded to the molybdenum atom (Mo=O). Therefore, three kinds of structurally different lattice oxygens exist, i.e., terminal oxygen

* Corresponding author. Tel.: +33 321 791 750; fax: +33 321 791 717.
E-mail address: sayede@lens.univ-artois.fr (A.D. Sayede).

0301-0104/$ - see front matter © 2005 Elsevier B.V. All rights reserved.
doi:10.1016/j.chemphys.2005.04.036

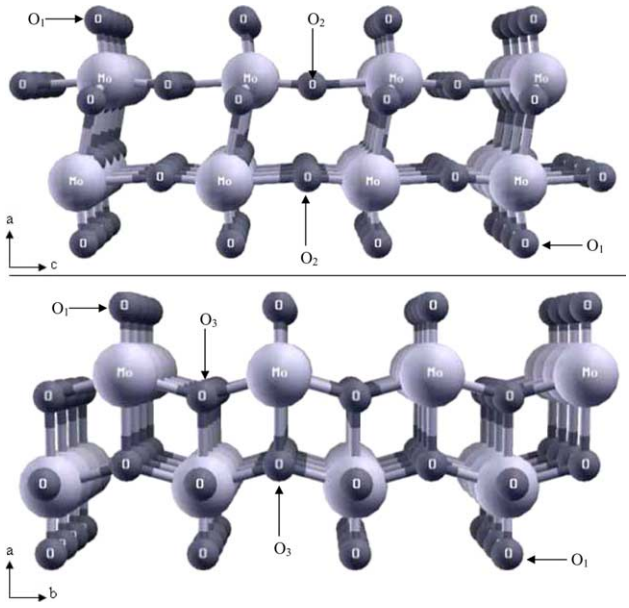

Fig. 1. Crystal structure of α-MoO_3.

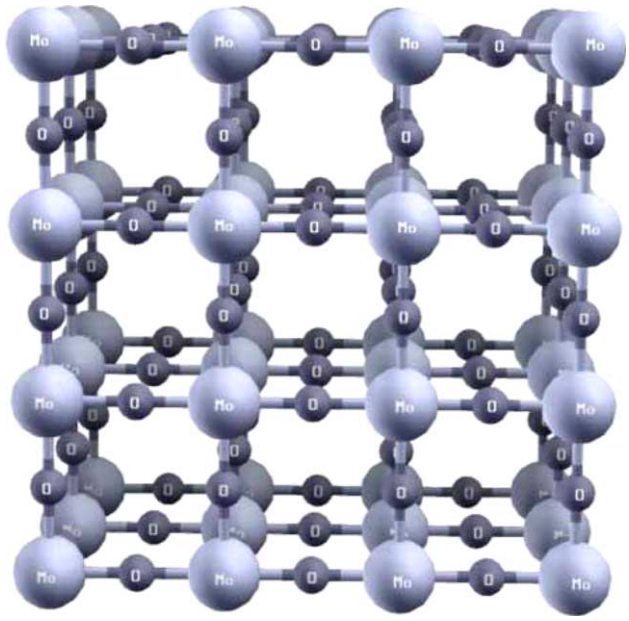

Fig. 2. Crystal structure of β-MoO_3.

(singly coordinated, O_1), asymmetric bridging oxygen (doubly coordinated, O_2, O_2'), and symmetric bridging oxygen (triply coordinated, O_3, O_3'). The MoO_3 layers are parallel to the (1 0 0) crystal plane, such as, the inter layer interaction is weak, and hence the (1 0 0) plane is the most exposed and thermodynamically most stable, where only O atoms are exposed on the surface. β-MoO_3 is similar to WO_3 and is related to the three-dimensional ReO_3 structure [13], which consists in corner-connected octahedra network, as shown in Fig. 2. It crystallizes with lattice constants $a = 7.122$ Å, $b = 5.366$ Å, $c = 5.566$ Å, and $\beta = 92.01$. The $\beta \rightarrow \alpha$ transformation is both exothermic and photochromic, with yellow β-MoO_3 converting to the white α phase above 400 °C at moderate heating rates [13]. The relatively high-transformation temperature implies that β-MoO_3 ought to have a fair measure of kinetic stability at or near room temperature. Nevertheless, X-ray diffraction measurements have shown that α-MoO_3 can be stabilized in the ReO_3 structure (β-MoO_3) by partially substituting molybdenum by tungsten [14].

Many applications of the molybdenum trioxide are prepared in thin film form [17]. A micro-Raman spectroscopy characterization [18] has shown that the films are almost composed by the β phase or (and) splashed species which consist of a mixture of the α and β phases. In addition, β phase has been a subject of deeper spectroscopic study [19]. In this study, the authors have shown that this photochromic material is promising in the areas of color displays and camouflage applications. Despite these applications and the more general importance of the β-MoO_3, both experimental and theoretical studies are still lacking. In contrast, α-MoO_3 has been the subject of many experimental [2–12] and theoretical [20,21] studies with respect to their structural and electronic properties (Note that the amount of theoretical work still few compare to the experimental one). In order to fill this gap, we initiated the present study. In doing so, we aim in particular to investigate the forces involved in the bonding between metal and oxygen and to understand why the β structure is metastable.

In this paper, both MoO_3 phases are studied using a periodical boundary condition ab initio LAPW method. In Section 2, we describe briefly computational details and Section 3 presents results and discussion. Finally, we summarize our conclusions in Section 4.

2. Computational details

The detailed geometries of both MoO_3 phase are obtained, in the present calculations, from total energy optimization, where the experimental structure for the orthorhombic structure is used as a starting point for the α phase [12]. The monoclinic phase has much more degrees of freedom than the α phase, and hence requires much more computing power for the structural optimization. We have therefore, chosen as a model system, the pseudo cubic structure (defect perovskite or ReO_3 like structure) suggested by McCaron in his initial description of this MoO_3 form [13]. This kind of approximation has been already used for the monoclinic WO_3 structure, which has been well described with the cubic ReO_3 like type structure [22,24]. To check this approach, we have compared the calculated band gap of the optimized cubic structure with the calculated band gap of the experimental monoclinic structure. It was found that the calculated band gap for the pseudo-cubic structure is

too much close to the monoclinic one (see Section 3). This allows us to use the pseudo-cubic system (instead of monoclinic structure) like a model able of reproducing the electronic structure of the β phase. For the two kinds of structures, the lattice constants are determined by lattice scaling such that the total energy of the unit cell is smallest. As next step, the position of all 16 atoms, in the optimized orthorhombic unit cell, are allowed to relax according to the force field (computed from total energy gradients) acting on the corresponding nuclei. In the cubic structure, this is not necessary because the structure does not contain internal degree of freedom. The system is supposed to be at the equilibrium if all force components are smaller than 0.1 mRy/Bohr. Ideally, the present two-step optimization has to be repeated iteratively until geometric self-consistency is obtained. However, the non-self-consistent optimization procedure has been tested in its accuracy and applied successfully to numerous systems, see e.g., [25]. It is adopted in the present calculations for computational convenience and is substantiated by the good agreement between theoretical and experimental geometries described in Section 3. The electronic structures of both MoO_3 phase are calculated within the density functional theory (DFT) formalism [26], using the gradient corrected functionals (GGA) for exchange and correlation [27]. Total energies and derived quantities are obtained with ab initio linearized augmented plane-wave (LAPW) method [28]. In LAPW procedure wave functions, charge density and potential are expanded in spherical harmonics within non-overlapping atomic spheres of radius R_{mt} and in plane waves in the remaining space of the unit cell [29]. The maximum angular momentum l for the waves inside the atomic spheres was confined to $l_{max} = 10$. The wave functions in the interstitial region were expanded in plane waves with a cutoff of $k_{max} = 8/R_{mt}$. The muffin-tin radius R_{mt} was 1.725 a.u. for Mo atoms and 1.5 a.u. for the O atoms. Extended test calculations have proven to yield sufficient accuracy in the total energy minimization of the β phase using 35 k points and of the α phase using 6 k point inside the irreducible part of the Brillouin zone. Respective densities of states (DOS) are evaluated with 48 k points for the α phase and 56 k points for the β phase inside the irreducible part of the Brillouin zone while the detailed band structure is based on 126 k points for the α phase and 131 k points for the β one along the high-symmetry direction.

3. Results and discussion

3.1. Geometric structure

The computed lattice constants for orthorhombic MoO_3 are listed in Table 1, together with data from experimental analysis. A comparison shows that the calculated constants are larger than 4% in respect to the experiment. Error on the distances between molybdenum atoms and the different oxygen atoms is less than 0.03 Å compared to the experimental values. This confirms the good agreement of our theoretical structure with experiment. Results from the structure optimization of cubic MoO_3 are also included in Table 1. Here, the computed lattice constant is compared with the pseudocubic lattice constant cell. The calculated total energy of cubic MoO_3 displays a minimum for a lattice constant of 3.827 Å. Thus, the calculated equilibrium volume is in good agreement with experiment.

Table 1
Calculated and experimental structural data for both MoO_3 phases

α-MoO_3	Obs. [12]	Corà et al. [20]	This work
a (Å)	13.855	14.271	14.577
b (Å)	3.696	3.680	3.744
c (Å)	3.963	3.910	4.021
Mo(x)	0.1016	0.0956	0.0978
Mo(z)	0.0867	0.0887	0.0867
$O_1(x)$	0.2214	0.2113	0.2124
$O_1(z)$	0.0373	0.0483	0.0341
$O_2(x)$	0.0866	0.0841	0.0858
$O_2(z)$	0.5212	0.5182	0.5193
$O_3(x)$	0.4351	0.4417	0.4379
$O_3(z)$	0.4994	0.5124	0.5075
Mo–O_1 (Å)	1.671	1.643	1.683
Mo–O_2 (Å)	1.734	1.687	1.748
Mo–O_2' (Å)	2.251	2.237	2.288
Mo–O_3 (Å)	1.948	1.937	1.969
Mo–O_3' (Å)	2.332	2.212	2.361

β-MoO_3	Pseudocubic [13]	This work
a (Å)	3.900	3.827
Mo–O (Å)	1.950	1.914

The index used for labelling the oxygen atoms refers to their coordination in the crystal structure; oxygens with the same coordination number but at different distance from Mo ion in the MoO_6 coordination octahedron have been labelled with prime.

3.2. Charge distribution

In order to characterize the local charging in orthorhombic MoO_3, the spatial distribution of valence electrons inside the elementary unit cell is examined. Contour maps of the difference between the charge density of the self-consistent calculation and that of a superposition of respective free-atom charge are presented in Fig. 3(a) and (b). The anisotropy in the bonding is quite evident in the maps; in particular, we note that the two short bonds Mo–O_1 and Mo–O_2 display a significant increase of charge density in the bonding region typical of covalent interactions (charge flow from the metal center toward the oxygen), which is not present in the longer Mo–O_2', Mo–O_3 and Mo–O_3' bonds. To stress further the anisotropy of the bonding, we report in Fig. 4 the electron density profile along the five

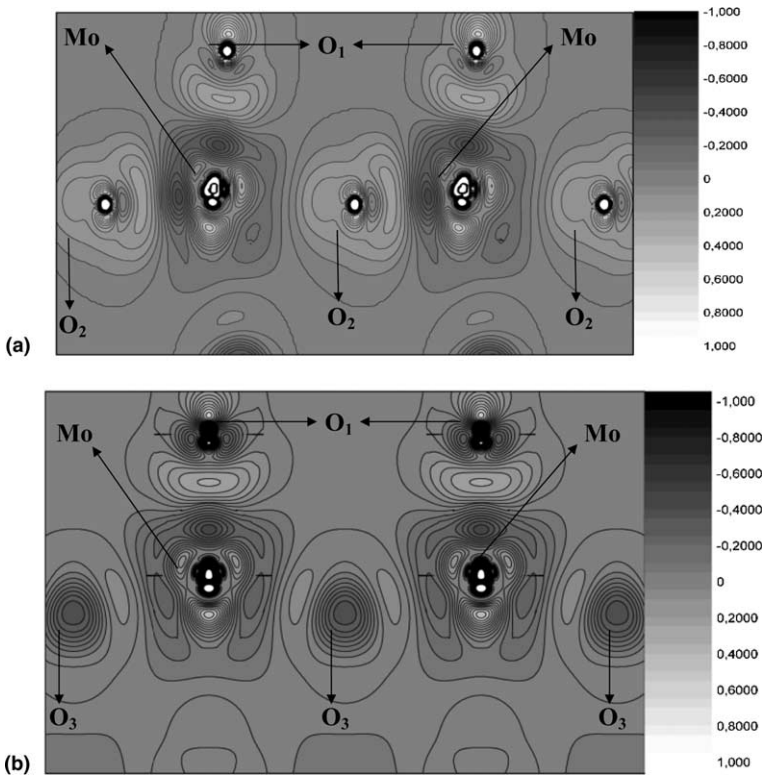

Fig. 3. Difference electron density of α-MoO_3 in the (a) (0 1 0) plane, and (b) (0 0 1) plane with respect to a superposition of respective free-atom charge. The contours refer to increments of 0.05 e/Å^3.

Mo–O bonds. The plot shows a very strong dependence of the electronic redistribution on the bond length. The accumulation of electron charge in the internuclear region, which characterizes covalent bonds, is clear for the short Mo–O bonds (0.180 e/Å^3 for Mo–O_1 and 0.130 e/Å^3 for Mo–O_2), while for the longer bonds we observe a polarization of the ions. In this case, the electronic charge is close to the atomic centers and therefore must be attributed to the ions, rather than shared in the central region. On increasing the equilibrium distance, there is an increasingly pronounced redistribution of charge towards the atoms. To quantify the information given in Figs. 3 and 4, we have reported in Table 2 the partial charge difference inside the atomic spheres. The difference charge is obtained by subtracting starting superposed atomic charge from the crystal converged LAPW charge. In the LAPW formalism, space is partitioned in two types of region, namely the spheres around the atoms and the interstitial regions, where different basis set expansions are used [29]. Due to this spatial decomposition, part of the electronic charge falls in the interstitial region, where it cannot be assigned to a particular atom. Partition of charge into partial charges is not unique and is always model-dependent. Note that the given charges within the atomic spheres are not comparable to usual ionic charges. Nevertheless, the electronic charge inside sphere surrounding the atomic nucleus can be helpful to discuss trends, bond properties and charge transfer between atoms. From Table 2, we can observe that there is a charge transfer from metal centers toward oxygen centers of about 0.412 electrons for the α case, where the O_3 bears the largest charge. This confirm the result deduced from Fig. 4. As known, larger distance lead to more oxygen charges and, therefore, more ionic character. Hence, the α-MoO_3 is a mixture of covalent and ionic character. The same feature is observed in our previous Hartree–Fock calculations [30] and in cluster calculations [31] performed for the (0 0 1) surface.

Fig. 5 represents the charge density plot on (1 0 0) plane and the electron density profile along the Mo–O bonds for the β phase. From these plots, it is clear that the bonds in β phase seems to be similar to the Mo–O_3 bond of the α phase. Indeed, the two bonds have closest length (1.96 and 1.91 Å for the α and β phase, respectively) and closest charge density (of about 0.08 electrons/Å^3) at the middle of the bond. Hence, we can conclude that the β-MoO_3 seems to be more ionic than the α-MoO_3 which has a mixed covalent-ionic character. This can be also seen from Table 2, where a much more charge transfer from metal centers toward oxygen centers (of about 0.582 electrons) is observed in the β structure comparatively to the α structure.

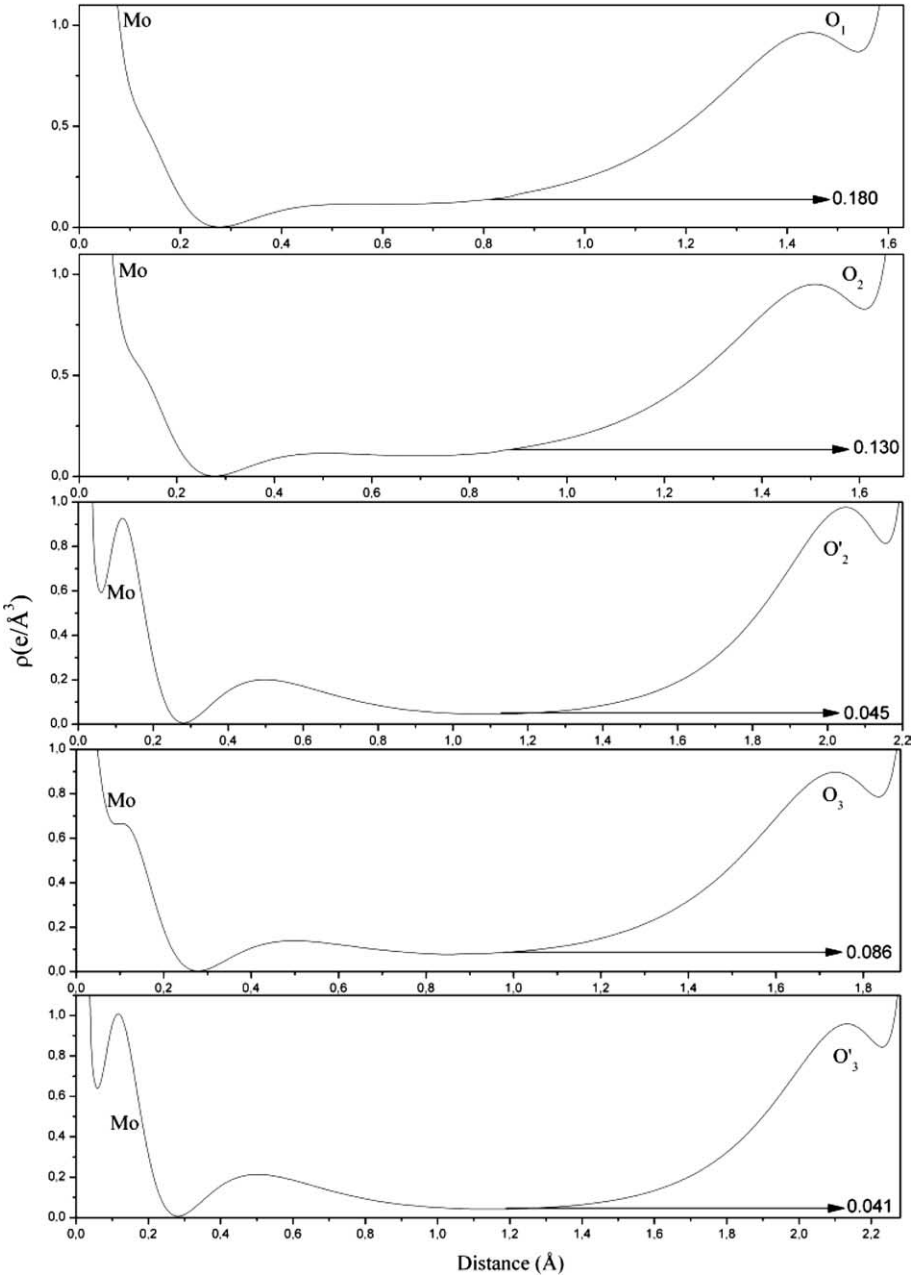

Fig. 4. Valence charge density profile for α-MoO_3 along the different Mo–O bonds. The values indicated by arrows represent the charge density values at the middle of the bonds.

Table 2
Partial charge difference of several valence bands inside the atomic spheres for both MoO_3 phases

Difference charges	α-MoO_3	β-MoO_3
ΔQ(Mo)	−0.412	−0.582
$\Delta Q(O_1)$	+0.197	
$\Delta Q(O_2)$	+0.251	+0.274
$\Delta Q(O_3)$	+0.363	

The difference charge is obtained by subtracting starting superposed atomic charge from the crystal converged LAPW charge. All entries are in number of electrons. We point out that in the case of β-MoO_3 there is only one type of oxygen.

3.3. Electronic structure

The electronic structures of the α and β-MoO_3 are characterized by energy bands and density of state (DOS) inside the irreducible part of the orthorhombic Brillouin zone as reported in Figs. 6–10. The Fig. 6 shows the calculated band structure of the α phase, where all energy values are taken with respect to the Fermi level such that negative energies refer to valence bands while positive values characterize conduction bands. The band structure consists of low-lying bands

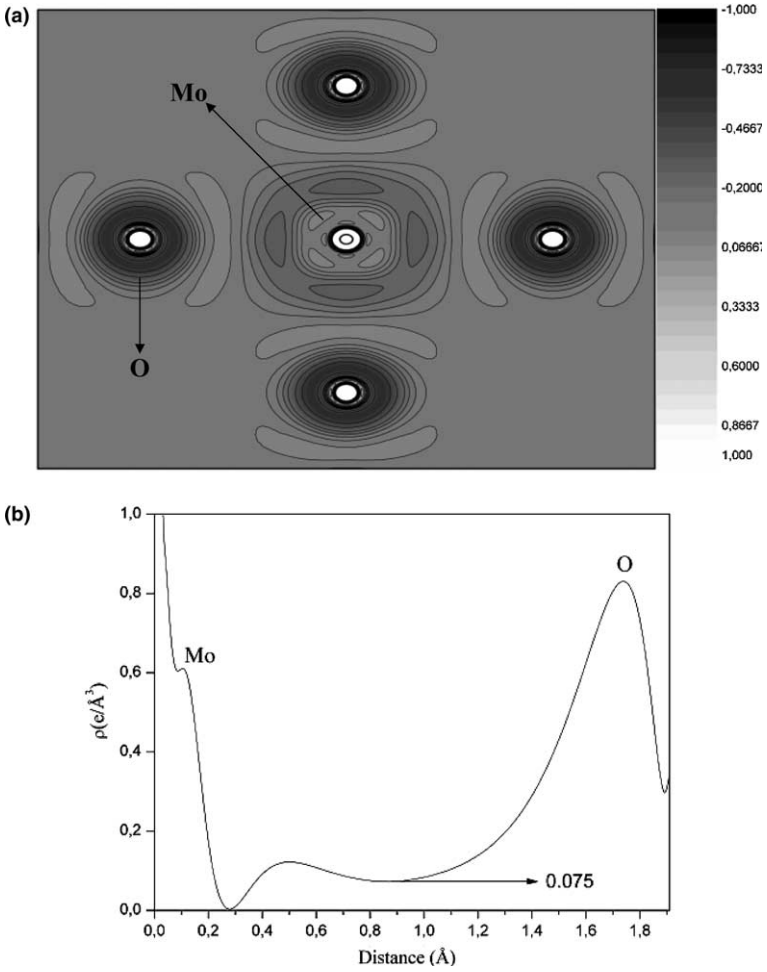

Fig. 5. (a) Difference electron density of β-MoO_3 in the (100) plane with respect to a superposition of respective free-atom charge. The contours refer to increments of 0.05 e/Å^3. (b) Valence charge density profile for β-MoO_3 along Mo–O bond.

originating from the O(2s) states at about 15–18 eV below the top of valence band (not reported in Fig. 6). The valence bands have a width of about 5.60 eV and the conduction bands are separated from valence bands by a gap of 2.23 eV which is more reasonable than the reported Hartree–Fock gap of 12.4 eV [20]. Using

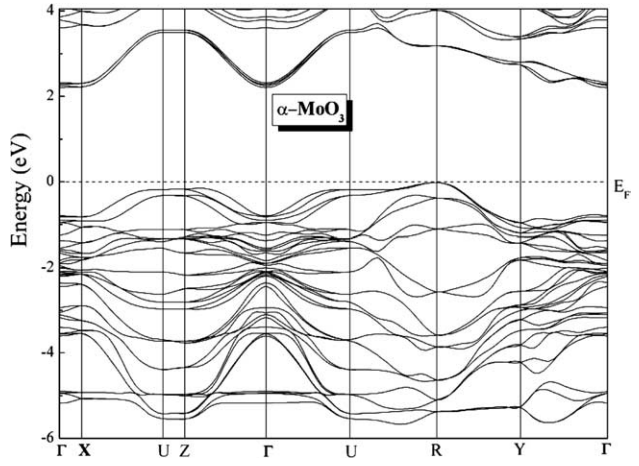

Fig. 6. Valence and conduction band structure for α-MoO_3 in a typical orthorhombic reciprocal space path, all the high-symmetry positions of the first Brillouin zone. All energies $\epsilon(k)$ are taken with respect to the fermi energy.

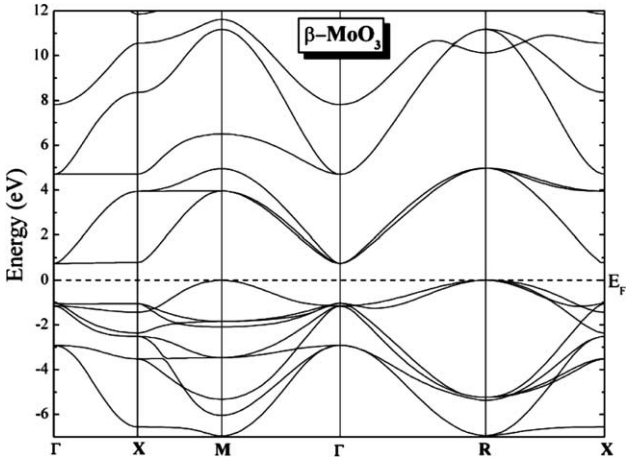

Fig. 7. Valence and conduction band structure for β-MoO_3 in a typical cubic reciprocal space path, all the high-symmetry positions of the first Brillouin zone. All energies $\epsilon(k)$ are taken with respect to the fermi energy.

TB-LMTO calculations in LDA, Rozzi et al. [21] reported a value of 0.5 eV. The experimental energy gap is about 3.3 eV [32]. Note that gaps are underestimated in DFT calculation and often have about a half of the experimental value. The low top valence bands (from −1.8 to −5.6 eV) show a more appreciable dispersion in k-space than the high top valence bands (just below the Fermi energy). This effect is typical of a covalent interaction as discussed in [33]. The flat bands at high top valence bands were attributed to the unshared electron pairs on the oxygen ions (as show by the PDOS of Fig. 10). The calculated band structure for β-MoO_3 is shown in Fig. 7. We note that the band structures sketched here are topologically very similar compared to those reported for the cubic WO_3 [23,24]. The oxygen 2s bands are centered at ≈18 eV below the Fermi level and have bandwidth of 1.67 eV. The valence bands have a width of about 6.95 eV and the conduction bands are separated from valence bands by a gap of 0.74 eV. This value is closed to the calculated band gap (1.01 eV) of the monoclinic structure (with experimental parameters). We are not aware of any published values of the β-MoO_3 bandgap. Furthermore, the approximation of the crystal structure (pseudo-cubic) used in the present work to model the β-MoO_3 phase, seems to be a good enough to reproduce the electronic structure of this compound. The band gap value of β-MoO_3 is quite small in comparison with that of the α-MoO_3. Similar band gap values were reported by LDA calculations in the case of the cubic WO3 [23,24]. These works also showed that displacement of the transition metal from its centro-symmetric position towards an oxygen ion causes increased hybridization of the transition metal W(5d) orbitals at the bottom of the conduction band

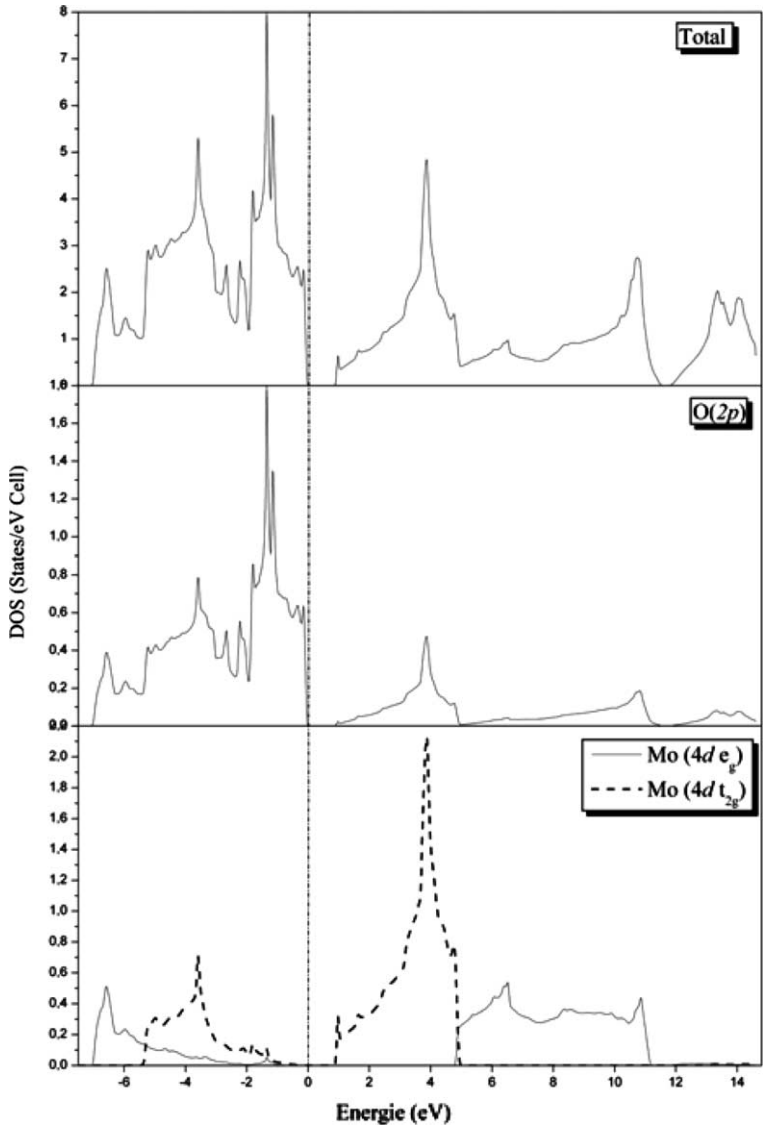

Fig. 8. Density of states (DOS) for β-MoO_3. Filled states are found at energies below zero and empty states above. Also are shown the O 2p, Mo 4d(t_{2g}) and Mo 4d(e_g) projected state densities.

with the O(2p) orbitals at the top of the valence band. This in turn lowers the energy of the top of the valence band and raises that of the bottom of the conduction band, explaining why WO3 has an off centering distortion. A similar effect could be observed when moving from the cubic MoO_3 structure to the orthorhombic one. Indeed, in this case, one of the metallic centers move toward two of its neighboring oxygens (O_1 and a little less toward O_2) and both valence and conduction bands are distorted (with bonding character in the valence band and antibonding in the conduction band); in particular, we observe a destabilization of the conduction band; for instance, the conduction band in the Γ–X direction that lies in the region of 0.74 eV (in the β-MoO_3) is destabilized by 1.47 eV (in the α-MoO_3).

The total valence DOS can be decomposed into local (inside the atomic sphere) partial (l-like) DOS according to the LAPW method, in which corresponding representation of the wave function is used. Together with the total DOS, in Figs. 8–10, we show the contribution due to single atoms and to the orbitals of molybdenum and oxygen of the α and β-MoO_3. For the β-MoO_3 compounds (Fig. 8), we observe that the valence band has a dominant contribution from the anion, while the conduction band has a higher contribution from the cation. This feature is typical of highly ionic system. However, an appreciable mixing of Mo and O orbitals can be noticed at valence and conduction band levels. One of important feature that can be observed from the PDOS concerns the metal e_g and t_{2g} contribution. In contrast to ideal cubic phase systems, at the valence band, the dominant contribution of t_{2g} levels is located at higher level (from E_F to −5.4 eV) where the dominant contribution of e_g levels is at lower energies (from

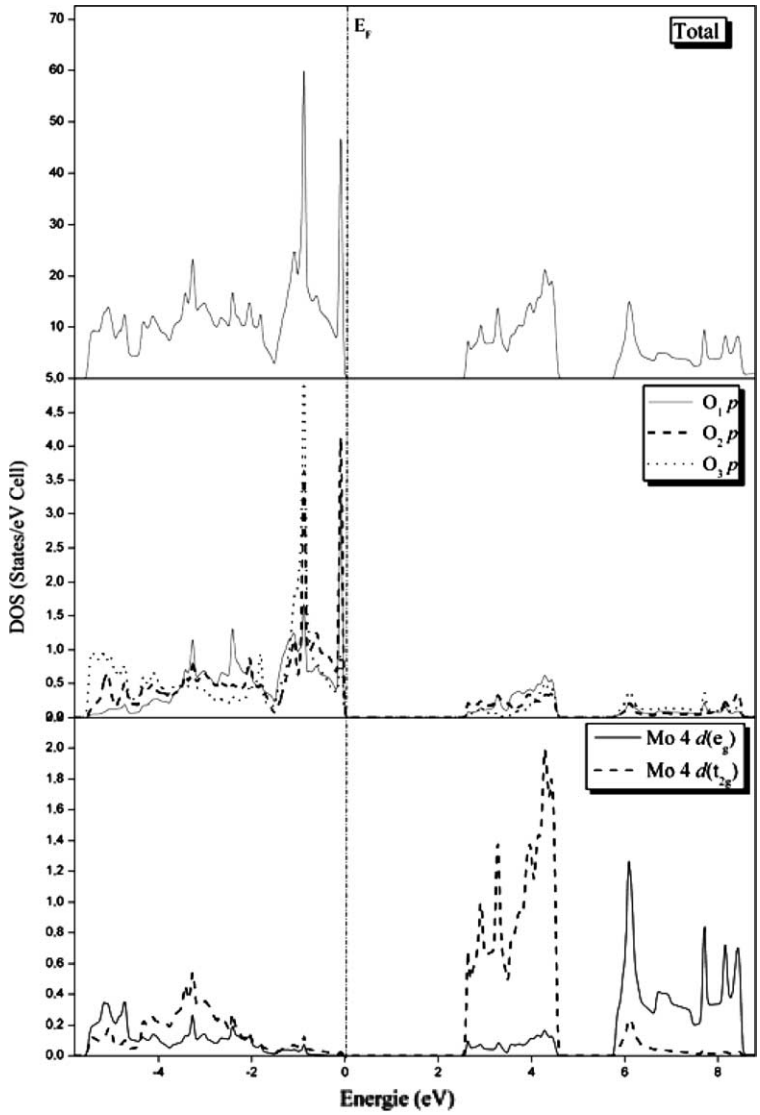

Fig. 9. Density of states (DOS) for α-MoO_3. Filled states are found at energies below zero and empty states above. Also are shown the O 2p, Mo 4d(t_{2g}) and Mo 4d(e_g) projected state densities.

−5.4 to −7 eV). The back-donation effect transferring electrons from oxygen toward metal centers causes a minor mixing between the metal and oxygen levels, the interaction is most effective for e_g levels pointing directly towards the nearest neighbors oxygens that is for the t_{2g} levels. This is why those latter appear at higher energies than the e_{2g} levels in the valence band. This characterizes generally a covalent contribution. Hence, the β trioxide molybdenum seems to be not a pure ionic system and has a minor covalent contribution to the bonding. When moving from the cubic phase (where the transition metal is octahedrally coordinated by oxygen) to the orthorhombic one (where the symmetry of the perfect octahedron is broken), we find that the different oxygen atoms have distinct, but similar PDOS in the valence region. The valence band appears to be split into two sub-bands: one just below the Fermi level (Fig. 9) has contributions from the oxygen atoms (the unshared electron pairs), but very small component from the metal. The lower sub-band (from −1.4 to 4.18 eV) has, in contrast, appreciable contributions from both metal and oxygen. As mentioned before, effects of this kind are typical of covalent contributions [33]. We observe also that the conduction band is split-off into two bands separated by a gap of about 1.12 eV. Due to the reduction of the local symmetry at the Mo sites, an appreciable but finite e_g–t_{2g} configuration mixing is observed.

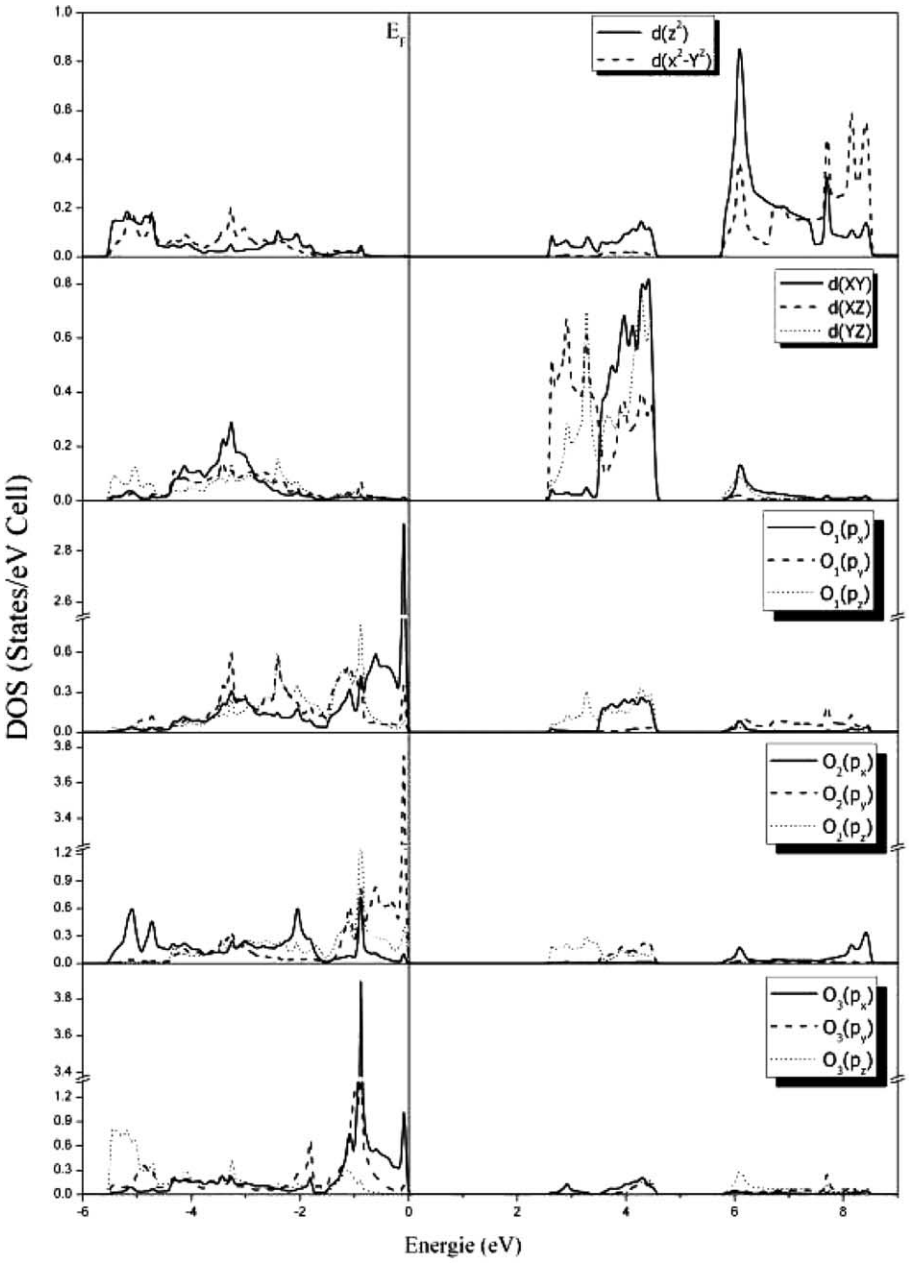

Fig. 10. Partial Mo 4d(t_{2g}), Mo 4d(e_g) and O(2s) DOS of α-MoO_3.

We display in Fig. 10 the partial DOS of the Mo(4d t_{2g}), Mo(4d e_g) and O(2p) states resolved into their symmetry components in the α phase. Turning to the e_g derived band first, we mention the presence of double peak structure of the Mo($4d_{z^2}$) and Mo($4d_{x^2-y^2}$) partial DOS in the interval between −5.5 and −4.6 eV. The shape of the Mo($4d_{z^2}$) peak around −5.4 eV resembles to the $O_3(p_z)$ DOS and thus indicates the p–d hybridization. The peak around −5.1 and 4.7 eV, in contrast, is derived mainly from overlap of the Mo($4d_{x^2-y^2}$) states with $O_2(p_x)$ states and, to a much lesser degree, with the $O_1(p_y)$ states. The peak around −3.2 eV derived from overlap of the Mo($4d_{x^2-y^2}$) and the $O_1(p_y)$ states and, to a half degree, $O_1(p_x)$ and $O_2(p_y)$ states.

For t_{2g} states, which are responsible for the weaker π type overlap with the oxygen 2p states, we observe mainly two feature: (i) the peak at $\simeq$−3.2 eV in the Mo($4d_{xy}$) partial DOS results from hybridization with the $O_1(p_x/p_y)$ and $O_2(p_y)$ orbitals; (ii) the dominant Mo($4d_{yz}$) contribution in the energy region of $\simeq$−2.4 eV clearly indicates overlap with $O_1(p_y)$ and $O_1(p_z)$ orbitals. From these PDOS, we point out the existence of both σ and π bonding between Mo and O_1 atoms which lead to increase covalency of these bond, the same feature is observed for the Mo–O_2 bonding with much less magnitude. This behavior is caused by the Mo atoms shift toward the molybdenyl and O_2 atoms. We underlined the absence of hybridization involving Mo($4d_{xz}$) orbitals. This has as consequence a flat band structure along the *Γ–X* and *U–Z* directions.

Moving from the cubic to the orthorhombic structure. One can observe clearly the increase of the mixing between e_g and t_{2g} states. This indicate the increase of the covalence for the α phase. This feature has been observed during the octahedral deformations in the orthorhombic V_2O_5 [34]. One of the striking things in the non-cubic phase is the clear split-off of the conduction band where metallic orbitals are dominant. The PDOS of these orbitals show a minor mixing between Mo(4d t_{2g}) and Mo(4d e_g) states in the conduction band. This mixing is absent in the conduction band of the β phase. These two features can be used as distortion gauge of the MoO_6 octahedra. This distortion is responsible of covalency increase for Mo–O_1 and Mo–O_2 bonding and hence the stabilization of the MoO_3. This explains partly the stability of α phase comparatively to the β phase. The relatively large displacement of metal ion toward oxygen (O_1 and O_2), lead to the formation of oxomolybdenum cations, $(Mo{=}O)^{4+}$, which give birth to the thermodynamical stabilized 2D layered structure.

4. Conclusion

This theoretical study provides a detailed picture of the geometric and electronic structure of both phase of the trioxide molybdenum. Geometry optimizations of the orthorhombic MoO_3 based on LAPW calculations yield to lattice parameter values in agreement with experiment, the Mo–O bond lengths are very close to experimental values. Charge distribution results confirm the mixed ionic and covalent character of bonding in α-MoO_3. The symmetrically bridging oxygens exhibit more ionic feature while the terminal oxygens are more covalent. The lattice scaling of the β-MoO_3 gives results which are in excellent agreement with the reported experimental pseudo-cubic results. Mo–O bonding in this phase is similar to the Mo–O_3 bond of the α phase. Also, It was found, from PDOS, that β-MoO_3 is not a fully ionic system and some covalent contributions are still appreciable. This covalent contribution to the bonding seems to be derisory compared to the covalent contribution of the α phase. A comparison between the Mo(d_{eg}) and Mo(d_{t2g}) states of both phases can explain the structural difference between them. Indeed, the octahedral deformation yield to an increase of the covalency between the Mo–O_1 and Mo–O_2 bond. This is easily identified by coexistence of both σ and π bonding in the orthorhombic phase. The aim of the octahedral deformation is to stabilize the MoO_3 structure, this explains in part the metastability of the β-MoO_3 structure.

References

[1] C.N.R. Rao, B. Raven, Transition Metal Oxides, VCH, New York, 1995.
[2] H.K. Kung, in: B. Delmon, J.T. Yates (Eds.), Transition Metal Oxides: Surface Chemistry and Catalysis, Studies in Surface Science and Catalysis, vol. 45, Elsevier, Amsterdam, 1989.
[3] V.E. Henrich, P.A. Cox, The Surface Science of Metal Oxides, Cambridge University Press, 1994.
[4] E.R. Braithwaite, J. Haber (Eds.), Molybdenum: an Outline of Its Chemistry and Uses, Studies in Inorganic Chemistry, vol. 19, Elsevier, Amsterdam, 1994.
[5] C.J. Machiels, W.H. Cheng, U. Chowdhry, W.E. Farneth, F. hong, E.M. McCarron, A.W. Sleight, Appl. Catal. 25 (1986) 249.
[6] Z. Hussain, J. Electron. Mater. 31 (2002) 615.
[7] J.O. Besenhard, R. Schöllhorn, J. Power Source 1 (1976) 267.
[8] M. Sugawara, Y. Kitada, K. Matsuki, J. Power Source 26 (1989) 373.
[9] M.E. Sphar, P. Novac, O. Haas, R. Nesper, J. Power Source 54 (1995) 346.
[10] T. Tsumura, M. Inagaki, Solid State Ionics 104 (1997) 183.
[11] I. Juárez Ramirez, A. Martinez de la Cruz, Mater. Lett. 57 (2003) 1034.
[12] L. Kihlborg, Arkiv Kemi. 21 (1963) 357.
[13] E.M. McCarron, J. Chem. Soc., Chem. Commun. (1986) 336.
[14] E. Salje, R. Gehlig, J. Solid State Chem. 25 (1978) 239.
[15] J.B. Parise, E.M. McCarron, A.W. Sleight, Mater. Res. Bull. 22 (1987) 803.
[16] J.B. Parise, E.M. McCarron, R. Von Dreele, J.A. Goldstone, J. Solid State Chem. 93 (1991) 193.
[17] H. Dwain Coble, K. Hashimoto, A. Fujishima, Appl. Surf. Sci. 81 (1994) 175.

[18] E. Haro-Poniatowski, M. Jouanne, J.F. Morhange, C. Julien, R. Diamant, M. Fernández-Guasti, G.A. Fuentes, J.C. Alonso, Appl. Surf. Sci. 127–129 (1998) 674.
[19] T. He, J. Yao, J. Photochem. Photobiol. C: Photochem. Rev. 4 (2003) 125.
[20] F. Corà, A. Patel, N.M. Harrison, C. Roetti, C.R.A. Catlow, J. Mater. Chem. 7 (1997) 959.
[21] C.A. Rozzi, F. Manghi, F. Parmigiani, Phys. Rev. B 68 (2003) 075106.
[22] A. Hjelem, C.G. Granqvist, J.M. Wills, Phys. Rev. B 54 (1996) 2436.
[23] F. Corà, A. Patel, N.M. Harrison, R. Dovesi, C.R.A. Catlow, J. Am. Chem. Soc. 118 (1996) 12174.
[24] M.G. Stachiotti, F. Corá, C.R.A. Catlow, C.O. Rodriguez, Phys. Rev. B 55 (1997) 7508.
[25] X.G. Wang, W. Weiss, Sh.K. Shaikhutdinov, M. Ritter, M. Petersen, F. Wanger, R. Schlögl, M. Scheffler, Phys. Rev. Lett. 81 (1998) 1038.
[26] W. Kohn, K. Sham, Phys. Rev. A 140 (1965) 1133.
[27] J.P. Perdew, K. Burke, M. Ernzerhof, Phys. Rev. Lett. 77 (1996) 3865.
[28] P. Blaha, K. Schwarz, G.K.H. Madsen, D. Kvasnicka, J. Luitz, WIEN2k, An Augmented Plane Wave + Local Orbitals Program for Calculating Crystal Properties (Karlheinz Schwarz, Techn. Universität Wien, Austria), 2001. ISBN 3-9501031-1-2.
[29] D.J. Singh, Planewaves Pseudopotentials and the LAPW Method, Kluwer Academic, Boston, 1994.
[30] A. Sayede, B. khelifa, A. Aourag, C. Mathieu, J. Theo. Comp. Chem. 2 (2003) 245.
[31] R. Tokarz-Sobieraj, K. Hermann, M. Witko, A. Blume, G. Mestl, R. Schlgl, Surf. Sci. 489 (2001) 107.
[32] A. Bouzidi, N. Benramdane, H. Tabet-Derraz, C. Mathieu, B. Khelifa, R. Desfeux, Mat. Sci. Eng. B 97 (2003) 5.
[33] R.A. Wheeler, M.-H. Whangbo, T. Hughbanks, R. Hoffmann, J.K. Burdett, T.A. Albright, J. Am. Chem. Soc. 108 (1986) 2222.
[34] V. Eyret, K.-H. Höck, Phys. Rev. B 57 (1998) 12727.